Chemical Engineering Science 263 (2022) 118074

Contents lists available at ScienceDirect

Chemical Engineering Science

journal homepage: www.elsevier.com/locate/ces

Modelling of dispersed oil/water flow in a near-horizontal pipe

Jørn Kjølaas [a,*], Heiner Schümann [a], Diana Gonzalez [b], Stein Tore Johansen [a]

[a] SINTEF Industry, Norway
[b] Norwegian University of Science and Technology, Norway

HIGHLIGHTS

- A gravity-diffusion model for predicting water droplet concentration profiles in oil/water pipe flow was implemented.
- In the model, the droplet size distributions could be replaced by the Sauter mean values without loss of accuracy.
- The effect of turbulence of the droplet/fluid drag force was found to be important.
- In general, a good match between the model predictions and data was found, although there was room for improvement for the lowest flow rates.

ARTICLE INFO

Article history:
Received 26 April 2022
Received in revised form 21 August 2022
Accepted 6 September 2022
Available online 13 September 2022

ABSTRACT

A gravity-diffusion model was implemented for predicting water concentration profiles in dispersed oil-continuous oil–water flows. In this model, the measured droplet size distributions were used instead of a droplet size closure law. The turbulent diffusion was modelled assuming single-phase flow while the gravitational drift was based on closure laws from the literature, including hindrance effects. The results showed that including the effect of turbulence on the drag force was important, where the turbulent fluctuations cause an increase in the average drag because of the non-linearity of the drag law. The model yielded a good match with the experimental data reported by Gonzales et al. (Gonzalez et al., 2022), especially at the highest flow rates.

We also concluded that the following model simplification could be introduced without changing the results significantly:

1) The droplet size distributions could be replaced by the Sauter mean droplet size.
2) The diffusivity profile model could be replaced by a uniform diffusivity model.

1. Introduction

Multiphase flow has many application areas, and one area of particular importance is related to hydrocarbon transport from wells to the associated processing facilities. Here, the ability to predict the flow characteristics accurately is crucial for both design and operation of such systems. The increased focus on minimizing the carbon footprint of hydrocarbon transport systems has led to the proliferation of tie-back solutions, where new hydrocarbon assets are connected to existing infrastructure instead of building standalone installations. One of the main challenges with this approach is that the produced fluids must be transported over longer distances, which leads to larger uncertainties in the total pressure drop and flow stability. The development of these tie-back solutions thus requires simulation tools that are as accurate as possible to mitigate these uncertainties.

Oil-water flow is an important special case in the realm of multiphase flow. Oil transport lines often contains large water fractions, either because pre-separation of water is not feasible, or because water is injected to reduce the flow resistance (Joseph et al., 1997). It is then important to understand how the two phases interact, and how this influences the pressure drop. A good understanding of oil–water flow is also a prerequisite for predicting three-phase gas/oil/water flows, which is the most common scenario in hydrocarbon transport.

In many practical oil/water flow scenarios, such as petroleum production and transport, the fluids are transported over long distances (tenths of kilometres), and the simulation method must then be selected accordingly. Specifically, full 3D simulations are not feasible in such cases because of the computational cost, and a more pragmatic approach must then be applied. It is thus the aim of this paper to propose a model that contains the most

* Corresponding author.
E-mail address: jorn.kjolaas@sintef.no (J. Kjølaas).

https://doi.org/10.1016/j.ces.2022.118074

important physical phenomena for predicting dispersed oil/water flows, but at the same time make simplifications that can lessen the computational time for simulations.

There are many experimental studies of oil–water flows in the literature, but most of them do not have many detailed measurements (Kumara et al., 2009; Brauner, 2003; Yang et al., 2021; Santos et al., 2019). This is regrettable because to obtain a proper understanding of the mechanics of dispersed oil/water flows, simultaneous measurements of both phase fraction profiles and droplet sizes are needed. A few oil–water experimental studies include local phase fraction measurements, but with no droplet size measurements (Amundsen, 2011; Elseth, 2001; Soleimani, 1999). Although such phase fraction measurements are certainly very useful, the absence of droplet size measurements leaves the door open for model developers to tune the droplet size model to match the experiments. This droplet size tuning can very easily cover up other weaknesses in the modelling without the developer's knowledge, possibly leading to a model with several closure law errors that largely cancel each other out. Even if such a flawed model is shown to provide good overall predictions in one particular data set, there is every chance that it will not work in other situations. It is thus important that the closure laws used in flow simulation models are calibrated and validated independently.

To our knowledge, the oil–water pipe flow campaign conducted by Gonzalez et al. (Gonzalez et al., 2022) is the only study of its kind where both local phase fractions and droplet size were measured simultaneously in a sufficiently long test section (212 m) to reach developed flow. This data set thus provides a unique opportunity to make progress on the modelling of oil–water flows, and arguably also particle-laden flows, which is essentially the same type of situation. In this paper we have elected to focus on fully dispersed oil-continuous flow, where all the water is entrained as droplets in the oil phase. This flow regime is ideal for examining some of the most important physical mechanisms in oil–water flows, namely turbulent diffusion and gravitational drift.

There are some interesting works on the modelling of oil/water flows in the literature, and we will briefly describe some of them here. Amundsen (Amundsen, 2011) implemented a unified model for dispersed/separated oil/water flow based on a gravity/diffusion balance to describe the behaviour of the dispersed droplets. A tuned version of the Richardson-Zaki model (Richardson and Zaki, 1954) (described in Section 3.3) was used to account for droplet hindrance effects. Good agreement with the experimental data was reported. However, the droplet sizes were not known in the experiments, and the droplet size used to calculate the settling velocity was obtained by multiplying the maximum stable droplet size given by the Hinze model (Hinze, 1955) by 0.557.

$$d = 0.557 \cdot d_{\max} \tag{1}$$

where d_{max} is given by:

$$d_{\max} = 0.725\left(\frac{\sigma}{\rho}\right)^{0.6} \varepsilon^{-0.4} \tag{2}$$

Here, σ is the surface tension between the phases, ρ is the density of the continuous phase, and ε is the energy dissipation rate. It was pointed out that droplet size measurements would have been useful since the accuracy of the droplet size model was not known.

Paolinelli (Paolinelli, 2020) proposed a model for dispersed oil/water flow using the same modelling principle, i.e., a gravity/diffusion balance, and compared to phase fraction profiles reported in the literature. A normalized diffusivity of 0.255 was used, which is more than three times the generally accepted value for single phase flow (0.074) (Skartlien et al., 2011). Again, droplet size measurements were not available in any of the data sets, and the droplet size was calculated by multiplying the maximum stable droplet size given by the Hinze model (Eq. (2)) by the expression:

$$0.5(1 + K \cdot C) \tag{3}$$

where C is the volumetric droplet concentration K is a parameter taking on values in the range 3–5.4 depending on the droplet concentration. No droplet hindrance was considered in the model. The model was reported to give good agreement with measured phase fraction profiles. The phase fraction profiles were further used for predicting the transition between separated and dispersed oil/water flow, using the assumption that the transition took place when the maximum concentration exceeded the phase inversion point.

Pouraria et al. (Pouraria et al., 2021) performed CFD simulations of dispersed oil/water flows using ANSYS FLUENT (Fluent User's Guide Release 14, Washington, PA, USA: Ansys Inc., 2011). Droplet size distributions were calculated using a transient population balance model. The forces on the water droplets included drag, lift, turbulent dispersion, and virtual mass forces. The turbulence was modelled by employing the standard k-ε model. The predicted phase fraction profiles were compared to experiments with reasonable agreement. The droplet size model was validated against droplet size measurements, but those measurements were not from the experiments where the phase fraction profiles were recorded.

Berrio et al. (Berrio et al., 2021) also performed CFD simulations of oil/water flows, comparing to experimentally obtained phase fraction profiles. The droplet size distributions were calculated using a transient population balance model, but the droplet size supplied at the inlet was tuned for each case to obtain a best possible match with the phase fraction profiles.

Santos et al. (Santos et al., 2020) performed CFD simulations using COMSOL Multiphysics (COMSOL, 2019) in a 2D geometry using a Eulerian–Eulerian approach and the k-ε model for turbulence modelling. The droplet size was given a value of 120 μm. The predicted pressure gradients and phase fraction profiles compared favourably to experimental data. The phase fraction profiles were however completely homogeneous in all cases, making it difficult to assess the accuracy of the droplet dispersion model.

A common theme in all these modelling efforts is that the droplet sizes were not measured in the experiments, compelling the authors to use droplet size models found in the literature. Since the accuracies of those droplet size models are not known, the accuracies of the proposed closure laws related to the turbulent dispersion and gravitational drift cannot be assessed, because the overall agreement or lack thereof can always potentially be attributed to uncertainties in the droplet size model. Indeed, different authors have proposed widely different values for the normalized turbulent diffusivity, ranging from 0.049 (Amundsen, 2011) to 0.255 (Paolinelli, 2020) for systems that are very similar. We suspect that the main reason for these disparities has to do with uncertainties in the droplet size closure laws.

The primary novelty of this paper is that we have implemented a model for predicting phase fraction profiles that uses measured droplet size distributions instead of a droplet size model. This has not been possible before the paper by Gonzales et al. (Gonzalez et al., 2022) since there appears to be no previous oil/water experiments where both phase fraction profiles and droplets sizes have been measured simultaneously. The benefit of this is that we can focus on the modelling of the droplet dispersion process and gravitational drift, without worrying about uncertainties in the droplet sizes.

In the following sections we first provide a brief description of the experiments conducted by Gonzalez et al. (Gonzalez et al., 2022). We then propose a model based on a balance between turbulent diffusion and gravity using the measured droplet size distri-

butions instead of a droplet size model. Next, we simplify the modelling significantly by replacing the droplet size distributions with the Sauter mean droplet size, and by assuming a homogeneous turbulent diffusivity. Finally, we introduce a correction to the settling velocity model by including the effect of the turbulent velocity fluctuations.

2. Experiments

The oil–water pipe flow experiments used in this paper were conducted by Gonzalez et al. (Gonzalez et al., 2022) and we will briefly describe them here. The experiments were conducted in a stainless-steel flow loop with inner diameter D = 56.3 mm and total length of L = 212 m, and the pipe inclination was 0.13°. A schematic illustration of the flow loop is shown in Fig. 1. The oil phase used in the experiments was Exxsol D60, and the water phase consisted of tap water with 3.5 wt% sodium chloride. The thermodynamic properties of these fluids are listed in Table 1. The experiments cover mixture velocities U_M in the range 2–4 m/s, and water cuts WC = 5–38 %.

In the experiments shown in this paper, the oil/water flow regime is supposedly oil continuous, with water droplets dispersed in the oil. The flow regime assessment was done using conductance probes mounted on the pipe wall, which measure the local conductance in the immediate vicinity of each sensor. By comparing the measured values to values obtained with pure oil/water, we could assess if the continuous phase at the wall was either oil or water. This system is described in detail in (Gonzalez et al., 2022).

It should be noted that the conductance measurements were open to some interpretation, as the values obtained were usually somewhere in between the values for oil and water. We should also point out that in the experiments with U_M = 2 m/s and WC $\geq$ 20 %, we did observe conductance-values close to that of water at the bottom of the pipe, hence the flow regime for those cases might not have been fully dispersed. We have however nonetheless elected to include these experiments in the analyses.

The average Reynolds numbers of these experiments are in the range 10^4 to 10^5, which is well into the turbulent flow regime. At the lowest velocities (U_M = 2 m/s), the local volumetric water concentrations become high at the bottom of the pipe, potentially leading to high local effective viscosities because of emulsion effects (Pal and Rhodes, 1989), yielding Reynolds numbers lower than 10^4, but it was found that the flow was still turbulent in those circumstances.

2.1. Droplet size measurements

Droplet sizes were measured using a particle-sizing camera (CANTY InFlow™) near the outlet of the pipe (209.5 m from the inlet). The sampling tubes pointed opposite to the flow direction and could be traversed in the vertical direction, such that samples at different heights could be taken (0.8 cm from top, centre, 0.8 cm from bottom). The sampling tubes were connected to the particle-sizer taking in-situ videos of the passing droplets. The droplets were measured and counted using a machine learning algorithm based on an open-source code in TensorFlow.

The droplet counting obtained with the algorithm was verified by comparison with manual counting done with the program ImageJ. Three random experimental points were selected for the automatic counting verification. Based on previous experiences, at least 1000 droplets were manually counted for each video. Characteristic droplet diameters were estimated for the automatic and the manual counting, for the same test points, and compared against each other. The Sauter mean diameter obtained with the automatic counting, deviated from the manual counting by less than 7 %, for all the experimental points tested.

Fig. 2 shows some examples of the measured cumulative droplet size distributions. The size distributions shown here are volume-weighted, meaning that the distributions indicate the volume fractions of droplets within the respective droplet size ranges. Fig. 3 shows the Sauter mean droplet diameters plotted versus the water cut WC for mixture velocities U_M = 2, 3 and 4 m/s. For refer-

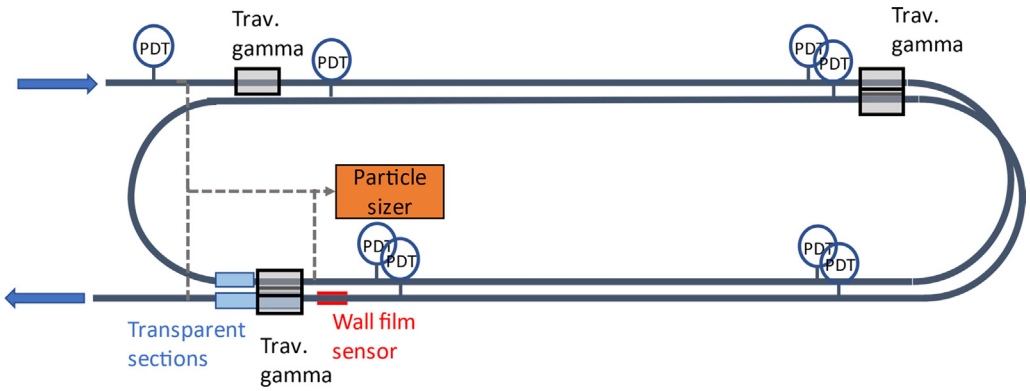

Fig. 1. Sketch of the test section and placement of instrumentation (Distances not to scale and instrument placements are just indications.) The symbols labelled "PDT" represent pressure transmitters, and the symbols labelled "Trav. Gamma" represent traversing gamma densitometers (see Section 2.2). The "particle sizer" box represents the equipment used to measure the droplet sizes.

Table 1
Fluid properties (IFT = Interfacial Tension).

Phase	Viscosity [kg/m3]	Density [kg/m3]	IFT – initial value [mN/m]	IFT – after 10 min [mN/m]
Oil	1.3	777	53.4	42.0
Water	1.0	1023		

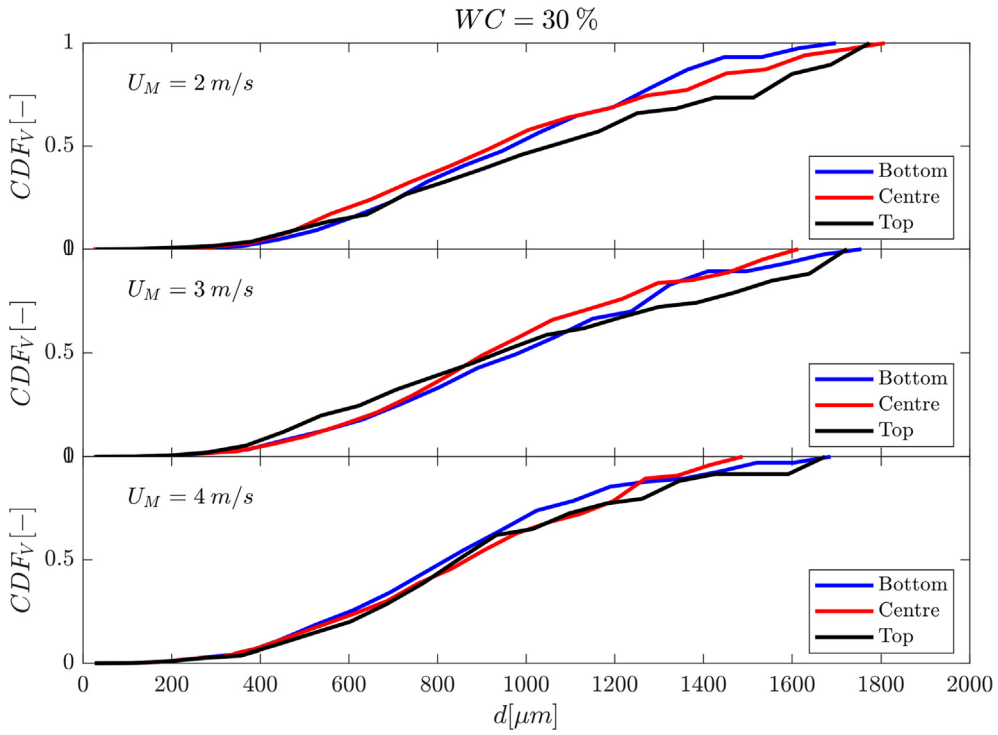

Fig. 2. Cumulative volume-weighted droplet size distributions for *WC* = 30 %.

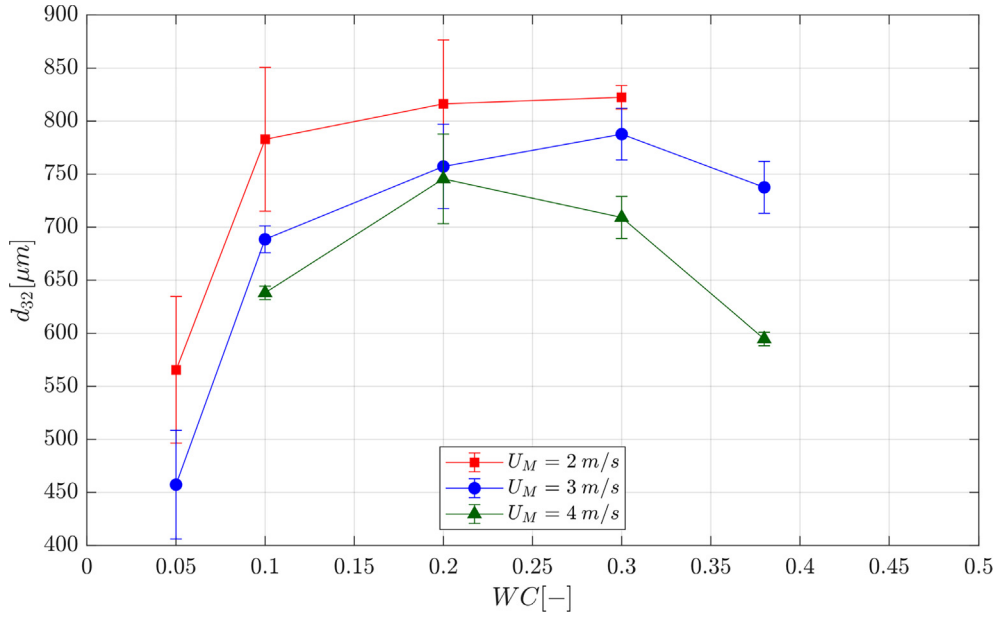

Fig. 3. The Sauter mean droplet diameter plotted against the water cut *WC*. The error bars represent the range of Sauter mean values measured at the three different vertical positions.

ence, the Sauter mean droplet diameter d_{32} is the area-weighted droplet diameter, and is defined as:

$$d_{32} = \frac{\langle d^3 \rangle}{\langle d^2 \rangle} \tag{4}$$

The error bars in Fig. 3 represent the range of Sauter mean values measured at the three different vertical positions.

2.2. Traversing gamma densitometers

Five vertically traversable gamma beam densitometers were used to non-intrusively measure cross sectional density profiles of the test section. In this paper we consider only the one at the end of the pipe, 206.7 m downstream of the inlet, about 5 m upstream the outlet. The liquid rates covered in this campaign were sufficiently high to preclude any unwanted outlet effects.

Indeed, even if the oil and water had been stratified (which was not the case), the flow velocities were too high to allow interfacial waves to travel in the opposite direction.

This gamma densitometer consisted of an Americium radiation source on one side of the pipe and a photon detector on the other side. The attenuation of the photon beam decreases exponentially with the density of the medium between the source and detector, yielding a measurement of the average density along the rays' travel path. In other words, the slice-average density is measured at each vertical position. By recording the photon count rates with pure oil and pure water in the pipe, the density profiles calculated in oil/water experiments were converted to water fractions, which is what we show in this paper. The gamma densitometer was logged at 50 Hz, scanning the pipe from bottom to top with a constant velocity of 0.2 mm/s. The associated results for all the experiments included in this paper are shown in Fig. 4.

The gamma densitometer data has a certain level of random noise originating from the stochastic nature of the photon emission process. This noise has a standard deviation of 0.05–0.06. In addition to this random uncertainty component, it is estimated that the measured values have an additional uncertainty with a standard error of about 0.015.

3. Modelling

To model the droplet concentrations presented in the preceding section, we have elected to use the classical steady-state gravity/diffusion equation, which has been deployed by numerous authors on problems related to the transport of particles in near-horizontal flows (Amundsen, 2011; Batchelor, 1966; Skartlien, 2009; Skartlien et al., 2011):

$$\varepsilon_P \frac{dC}{dy} + C \cdot U_T(C) = 0 \tag{5}$$

Here, C is the volumetric particle/droplet concentration, y is the vertical coordinate (normal to the flow direction), ε_P is the particle diffusivity, and U_T is the terminal velocity of the particles in the

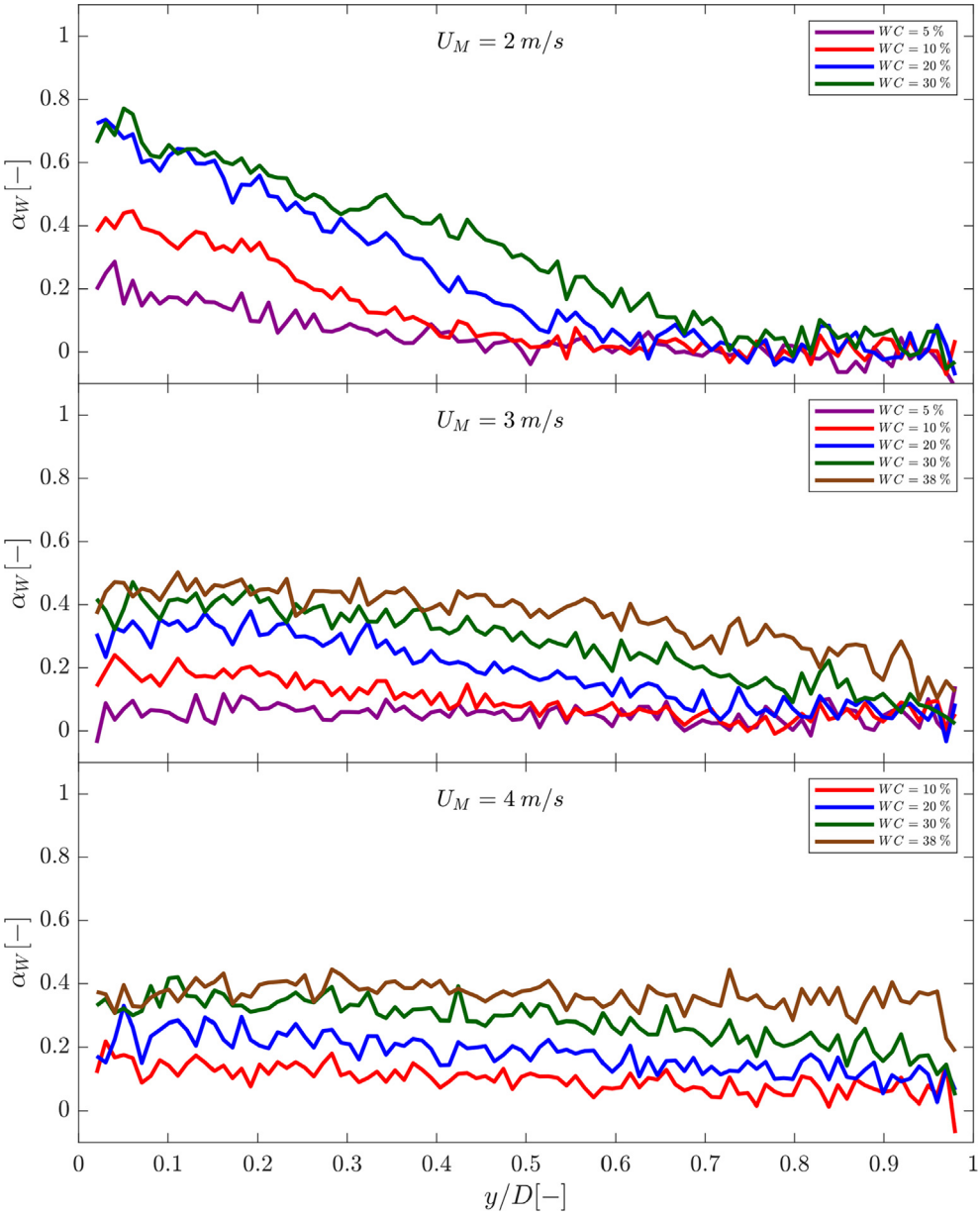

Fig. 4. Volumetric water concentration profiles measured by the traversing gamma densitometer near the end of the pipe. y/D = 0 represents the pipe bottom, and y/D = 1 represents the top of the pipe.

vertical direction relative to the liquid. The first term in Eq. (5) represents the average vertical particle flux due to turbulent diffusion of particles. The second term represents the average vertical particle flux due to gravitational drift, accounting for drag and hindrance effects. We have in this equation defined U_T to be positive, even though it points in the negative y-direction. In the remainder of this section we will use the terms "droplet" and "particle" interchangeably.

In the literature we have observed that some authors (Hunt, 1954; Karbelas, 1977; Paolinelli, 2020) have multiplied the second term by (1-*C*) on the grounds that this factor must be included to account for the upward displacement current induced by the falling particles. Our view is that including this term is incorrect because in the steady-state scenarios that are addressed here, the particle concentration is on average constant in time, hence there is on average no displacement current. However, as will be discussed in Section 3.4, large particle concentrations can cause significant interaction effects or hindrance, and this in fact compels the introduction of some similar amendments of the gravity term.

The gravitational drift of the droplets, here represented by the terminal velocity *UT* depends critically on the droplet size. In the model outlined in this paper, we have elected to use the measured droplet sizes instead of introducing a droplet size closure law. The proposed model is thus incomplete, but this approach allows us to investigate the other aspects of the modelling, without any concerns about the accuracy of the droplet size model. This has to our knowledge not been done before, as no previous oil/water flow studies in the literature have reported both phase fraction profiles and droplet size distributions for the same experiments.

The model described here assumes that the flow is fully dispersed, where the water is exclusively in the form of droplets dispersed in the oil, and the experiments included in this analysis have been selected accordingly. We assume that the axial water droplet velocity is equal to the local oil velocity. This assumption is supported by the fact that the average measured oil/water slip velocities in these experiments were close to zero, and that the deviations from zero slip could be attributed to measurement error. We also assume that the volumetric water concentration *C* is constant in the lateral direction.

When the flow is fully dispersed, we can solve Eq. (5) without introducing a boundary condition for *C*. Instead, we simply impose the condition of mass conservation in the axial direction. This is explained in more detail in Section 3.1.

In the following sections we start out by implementing a relatively detailed model for the volumetric droplet concentration, where the turbulent diffusion is modelled locally, and we also use detailed droplet size distributions to calculate the overall volumetric droplet concentrations. We then propose various simplifications, and we show that the simplified modelling gives essentially the same results as the detailed model. In the final section on the modelling (Section 3.6), we introduce a correction to the gravitational drift term, accounting for the effect of the turbulent velocity fluctuations on the average drag force.

3.1. Mass conservation

Assuming that the water phase is incompressible, mass conservation for the water droplets in the flow direction requires that the total volumetric water flux equals the supplied water flux *USW*:

$$USW = \frac{1}{A}\int_0^D C(y)\cdot U_x(y)dA \tag{6}$$

As noted previously, we have implicitly assumed that the volumetric water droplet concentration *C* is only a function of the vertical coordinate *y*, implying that *C* is constant in the lateral direction. We do not know how accurate this assumption is, so this may add some uncertainty in our model. However, without measurements of concentration profiles in the lateral direction, this seems like the only viable alternative.

The velocity profile $U_x(y)$ has been calculated assuming homogeneous turbulent flow, using the power law model:

$$U_x(r) = U_{MAX}(1-r)^{1/m} \tag{7}$$

Here, *r* is the dimensionless radial coordinate, and the parameter *m* has been calculated using the algorithm derived by Chen (Chen, 1990):

$$m = \kappa\cdot\sqrt{\frac{2}{f}} \tag{8}$$

where κ is the von Karman constant ($\approx$0.41), and *f* is the average Fanning wall friction factor, which was calculated from the measured frictional pressure gradient:

$$f = \frac{-(dp/dx)_{fric}\cdot D}{2\rho_M U_M^2} \tag{9}$$

The parameter U_{MAX} was subsequently calculated from mass conservation, i.e. that the velocity profile integrated over the pipe cross section equals the total volumetric flux:

$$U_M = \frac{1}{A}\int U_x(r)dA \tag{10}$$

The prevailing expression for U_{MAX} is then:

$$U_{MAX} = U_M\frac{(m+1)(2m+1)}{2m^2} \tag{11}$$

Based on the radial velocity profile $U_x(r)$, a slice-averaged velocity profile $U_x(y)$ was calculated numerically and used in the evaluation of the integral in Eq. (6).

We may note that while the "single-phase" velocity profile model applied here might not be entirely realistic in the presence of a heterogeneous droplet field, this does not seem to be too important for the sake of predicting droplet concentration profiles. Indeed, we tested the model using a completely flat velocity profile, and the results remained almost unchanged. However, as we point out in the next section, simplifying assumptions about the turbulence and the associated diffusivity may still have a negative impact on the predictions.

3.2. Eddy diffusivity and particle diffusivity

The driving force of the water droplet dispersion is the eddy diffusivity. There is an abundant literature on the topic of turbulent diffusion of particles, especially with respect to modelling particle deposition (Taylor, 1954; Reeks, 1983; Gudmundsson and Bott, 1977; Reeks, 1977; Vames and Hanratty, 2004; Hinze, 1972; Reeks, 1992; Johansen, 1991; Guha, 2008; Reeks, 2005; Pan and Hanratty, 2002). We must however be aware that the current work does not consider particle deposition since we are only modelling flows where all the droplets are dispersed. This is an important distinction because modelling particle deposition often revolves around getting the effective particle diffusivity in the wall boundary layer right. Indeed, the effective diffusivity of heavy particles tends to be elevated in the wall boundary layer because of inertial effects (Gudmundsson and Bott, 1977; Liu and Ilori, 1974). We will however show that the treatment of the boundary layer is not important for the modelling of our experiments, mainly because the boundary layer represents a relatively small part of the total volume of droplets.

For single phase fully turbulent flow, the eddy diffusivity is a relatively well-known quantity. Based on the measurements of

Nikuradse (Nikuradse, 1933); Reichardt (Reichhardt, 1951) derived a model for the local eddy diffusivity ε_F in single phase turbulent flow:

$$\frac{\varepsilon_F}{R \cdot U^*} = \frac{\kappa}{3}\left(\frac{1}{2} + r^2\right)(1 - r^2) \tag{12}$$

where R is the pipe radius, and U^* is the friction velocity:

$$U^* = \sqrt{\frac{\tau_{avg}}{\rho_M}} = \sqrt{\frac{D \cdot |dp/dx|_{fric}}{4\rho_M}} \tag{13}$$

Here, τ_{avg} is the average wall shear stress, ρ_M is the mixture density, and dp/dx_{fric} is the frictional pressure drop. This is the model that we have elected to use in this work, in addition to the simpler constant-diffusivity approach. It should be noted that in our model implementation we amended Eq. (12) by introducing a lower limit of 0.01, so that the local diffusivity at the wall did not reach zero. The exact choice of this lower limit is not critical with respect to the results, but a non-zero value at the wall is necessary to solve the gravity/diffusion equation. The expression derived by Reichardt can be viewed as universal in the sense that it is in principle valid for any single phase flow.

The dimensionless diffusivity obtained with Eq. (12) is plotted in Fig. 5. We observe that the values in the core region are around 0.07 and approaches zero at the walls. For reference, Vames & Hanratty (Vames and Hanratty, 2004) found that a reasonable value for dimensionless diffusivity in the Reynolds number range 10^4-10^5 was 0.074, which is close to the core values predicted by the Reichardt model. This value was confirmed by Young (Young and Hanratty, 1991). We can also mention that Biberg (Biberg, 2005) proposed a multiphase diffusivity model that is almost identical to the Reichardt model in the single phase limit.

In our case it is the particle diffusivity ε_P that is needed in Eq. (5), which is not necessarily the same as the eddy diffusivity ε_F. However, the most conventional approach to modelling the particle diffusivity is to assume that it is equal to the eddy diffusivity ε_F (Binder and Hanratty, 1992; Lee et al., 1989; Vames and Hanratty, 2004; Guha, 2008; Swailes and Reeks, 1994), and this is essentially the approach that we have used in the current work. This assumption is supported by the theoretical work conducted by Reeks (Reeks, 1977), as well as experiments conducted by Lee et al. (Lee et al., 1989); Vames & Hanratty (Vames and Hanratty, 2004), and Young & Hanratty (Young and Hanratty, 1991). Guha (Guha, 2008) showed that this assumption is adequate as long as other migration mechanisms, such as turbophoresis (Reeks, 1992) and lift forces (Saffman, 1965), are accounted for separately. We do however *not* believe these other migration effects to be important in the experiments examined in this paper. The reason is that these migration mechanisms are associated with the large velocity gradients near the pipe walls, and our results indicate that near-wall effects generally do not substantially impact the predictions.

The effective particle diffusivity can deviate from the eddy diffusivity when the particles are heavy compared to the surrounding fluid. Picart et al. (Picart et al., 1986) derived a model accounting for cross-trajectory effects, imposing a reduction in the particle diffusivity depending on the particle fluid slip:

$$\varepsilon_P = \frac{\varepsilon_F}{\sqrt{1 + \frac{0.85|\Delta U_P|^2}{2k_e/3}}} \tag{14}$$

In our case, ΔU_P is the average local particle–fluid slip velocity normal to the flow direction (i.e., the settling velocity), and k_e is the average turbulent kinetic energy per unit mass. In our model, k_e is approximated by:

$$k_e \approx \frac{3}{2}(0.9 \cdot U^*)^2 \tag{15}$$

The latter approximation may be called into question for the cases examined in this paper, where the droplet field is sometimes very dense. However, because the cross-trajectory effect is quite subtle in our cases, it is not necessary to include a more elaborate model.

This cross-trajectory effect was qualitatively confirmed by Young et al. (Young and Hanratty, 1991) who conducted experiments in a vertical pipe using steel spheres. The estimated dimensionless diffusivity was found to be 0.042 for the steel spheres, while the classical value of 0.074 was retained for glass spheres. For our cases, this amendment yields diffusivity corrections in the range 1–9 %, which is only barely noticeable on the prevailing results. We have however elected to include this contribution in our model.

We may also note that Reeks (Reeks, 1977) showed that the particle diffusivity can in principle exceed the eddy diffusivity in certain circumstances when the particle relaxation time is very long. This is however not the case for our experiments.

Skartlien (Skartlien, 2009) applied a slightly elevated value for the particle diffusivity compared to the eddy diffusivity in the modelling of gas/liquid flows with droplets to match the experimental data. However, a possible reason for why this increase in diffusivity was necessary may have been a weakness in the droplet

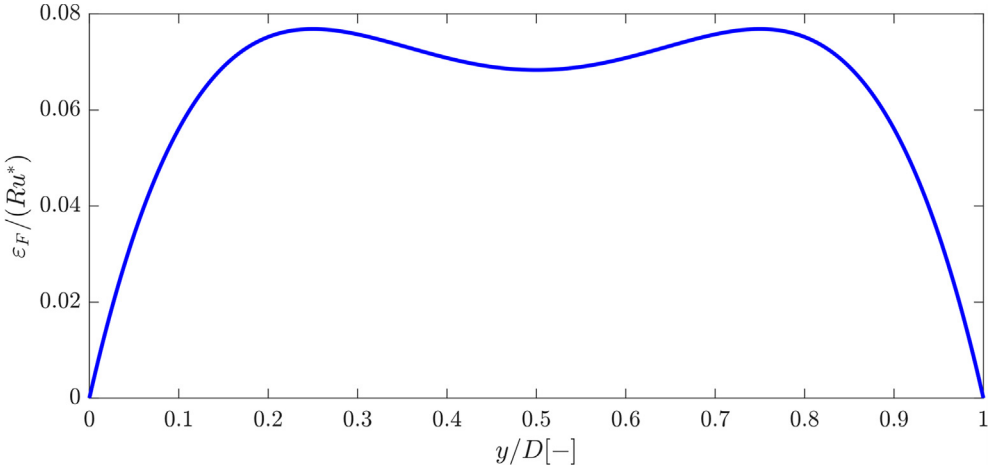

Fig. 5. The dimensionless diffusivity plotted versus the normalized distance from the pipe bottom, according to the model derived by Reichardt (Reichhardt, 1951). y/D = 0 represents the pipe bottom, and y/D = 1 represents the top of the pipe.

size model, as the droplet sizes were not measured in those experiments. Indeed, in a subsequent study on a similar data set, Skartlien (Skartlien et al., 2011) used a normalized diffusivity close to the classical value of 0.074.

Amundsen (Amundsen, 2011) conducted oil/water experiments similar to the ones presented in this paper, covering both dispersed and separated flow. Amundsen implemented a gravity/diffusion model that used a somewhat low value of 0.049 for the normalized diffusivity, but as in the cases with Skartlien (Skartlien, 2009; Skartlien et al., 2011), the droplet sizes were not known. Consequently, it is difficult to evaluate the legitimacy of this diffusivity value since errors in the diffusivity and droplet size may very easily cancel out.

For the experiments presented in Section 2, we assume that the particle diffusivity can be adequately modelled by assuming that it equals the eddy diffusivity, and the results shown in this paper arguably support this supposition. It should however be noted that we use a diffusivity model for single phase flow, which might not be accurate when the volumetric droplet concentration is high (Skartlien, 2007). However, since we do not have any measurements to support a more rigorous diffusivity model, we have elected to proceed with this simplified approach. It is however worth noting that this simplification may ultimately be a one of the most important limitations of the model because the turbulence can be affected by the presence of droplets. This is discussed in more detail in Section 3.6.

3.3. Terminal settling velocity in dense flows

Eq. (5) requires a closure model for the terminal settling velocity U_T. From a simple force balance between gravity, buoyancy and drag, the terminal velocity of a droplet with diameter d_D and density ρ_D immersed in a fluid with density ρ_F, is given by:

$$U_T^2 = \frac{4 d_D g_y (\rho_D - \rho_F)}{3 C_D \rho_F} \tag{16}$$

where g_y is the gravity acceleration in the y-direction, and C_D is the drag coefficient of the droplet. According to Haider & Levenspiel (Haider and Levenspiel, 1989), there are well over 30 different models for C_D in the public literature. However, the different models are mostly identical in form, differing only in the selected model coefficients. In this paper we have chosen the classical model proposed by Clift et al. (Clift and Weber, 1988) as the basis for this closure law:

$$C_D = 24 \frac{1 + 0.15 Re_D^{0.687}}{Re_D} \tag{17}$$

where Re_D is the particle/droplet Reynolds number:

$$Re_D = \frac{\rho_F d_D U_T}{\mu_F} \tag{18}$$

We use the term "basis" here because in dispersions that are densely populated with droplets, the terminal velocity given by these equations will severely over-predict the settling velocity. This is called the "hindrance" effect and is related to the notion that interactions between the droplets yields a lower average terminal velocity. This matter was investigated in detail by Richardson & Zaki (Richardson and Zaki, 1954), who derived an empirical formula expressing the relationship between the terminal particle velocity and the particle concentration:

$$U_T = U_{T0} \cdot (1 - C)^n \tag{19}$$

where U_{T0} is the terminal velocity at zero concentration, and n is a parameter that depends on the particle/droplet Reynolds number Re_D and the ratio between the particle diameter and the pipe diameter d/D. The latter dependency was attributed to wall effects in experiments where particles were settling in a vertical pipe. This effect is not relevant in our case because we are considering droplets falling in the direction normal to the pipe wall, hence we ignore this dependency in our model. Rowe (Rowe, 1987) showed that the expression suggested by Richardson & Zaki is adequately represented by the following formula:

$$n = \frac{4.7 + 2.35 \cdot K}{1 + K} \tag{20}$$

where

$$K = 0.175 \cdot Re_d^{0.75} \tag{21}$$

For the sake of simplicity, we will use the expression suggested by Rowe in this work, as the results will be undistinguishable from the original Richardson & Zaki model. For the calculation of U_{T0}, we use the drag coefficient given by Eq. (17).

An important note about Eq. (19) is that U_T in this case relates to the velocity of particles/droplets falling through a liquid column measured in the laboratory reference frame. When particles are in a static liquid column, there will be an upward displacement current of liquid balancing the downward particle flux, hence this settling velocity is not the same as the slip velocity between the particles and the liquid. The slip velocity ΔU_T is defined as the difference between the droplet settling velocity U_T and the surrounding fluid velocity U_F:

$$\Delta U_T = U_T - U_F \tag{22}$$

By multiplying this expression by (*1*-*C*), we get:

$$\begin{aligned}(1 - C)\Delta U_T &= (1 - C)U_T - (1 - C)U_F \\ &= U_T - [C \cdot U_T + (1 - C)U_F]\end{aligned} \tag{23}$$

The expression inside the right-most parentheses is the total mixture velocity in the vertical direction, which in our case is zero. This means that the relationship between the laboratory frame settling velocity U_T and the slip velocity ΔU_T is:

$$U_T = (1 - C)\Delta U_T \tag{24}$$

In Eq. (5), we are considering a steady-state situation where there is no net flux of particles in the vertical direction, and hence no net liquid flux either. Consequently, the contribution to U_T related to liquid displacement, which Richardson & Zaki included in their model, should not be included in our model. We must therefore replace U_T with ΔU_T in Eq. (5), where ΔU_T is given by:

$$\Delta U_T = U_{T0} \cdot (1 - C)^{n-1} \tag{25}$$

In other words, to adapt the Richardson & Zaki model to our system, we need to reduce the value of the model coefficient n by 1.

3.4. Detailed droplet concentration model

In this section we compare predictions obtained by solving Eq. (5) using the closure laws listed in the preceding sections. As previously noted, we use the droplet size distributions measured near the bottom of the pipe instead of using a model for the droplet sizes. The reason for using the bottom values is that we integrate Eq. (5) from the pipe bottom, and we thus need the droplet sizes there as a boundary condition.

We divide the measured droplet sizes into 15 bins with uniform bin widths, where the "height" of bin i equals p_i. Here the values of p_i represent the volume fractions of droplets at the pipe bottom, normalized such that $\sum_i p_i = 1$.

For simplicity we have assumed that there is no droplet coalescence or breakup. The gravity/diffusion equation for droplet size class i can then be written as:

$$\varepsilon_P(y)\frac{dC_i(y)}{dy} + C_i(y)\cdot U_{T0,i}\cdot\left(1-\sum_j C_j(y)\right)^{n-1} = 0 \quad (26)$$

We see that because of the Richardson & Zaki hindrance term (Richardson and Zaki, 1954), the equations for each droplet size class are coupled, which is rather inconvenient from a computational perspective. The numerical procedure that we used to solve this equation system was as follows:

1) Guess the total volumetric droplet concentration C_0 at the bottom of the pipe.
2) Calculate the bottom volumetric droplet concentration for each droplet size class i: $C_{0i} = p_i \cdot C_0$.
3) Integrate Eq. (5) for each droplet size class i with the boundary condition $C_i(0) = C_{0i}$.
4) Calculate the total concentration profile $C(y) = \sum_i C_i(y)$. If $C(y)$ changes significantly compared to the concentration profile obtained in the previous iteration, go back to step 3 until this change is sufficiently small.
5) Calculate the droplet volume flux for each droplet size class i using the approach outlined in Section 3.1 and add them together to yield the total droplet flux.
6) If the total droplet volume flux differs from the inlet water flux (USW), estimate a new value of C_0, and go back to step 2.

We will show in Section 3.6 that this somewhat elaborate algorithm can be greatly simplified by replacing the droplet size distributions with the respective Sauter mean droplet diameters. Specifically, with only one droplet size class we can skip steps 2 and 4 in the above algorithm.

Fig. 6 shows the volumetric water concentration profiles predicted by this model compared to the profiles measured using the last gamma densitometer for two experiments (WC = 20 % and U_M = 2, 3 and 4 m/s). We observe that the predicted profiles are quite close to the measurement for U_M = 2 m/s, while the model predicts a too heterogeneous profile for $U_M \geq 3$ m/s. We will return to this matter in Section 3.7.

3.5. Model simplifications

In this section we will explore ways of simplifying the model described in the previous sections. The motivations for simplifying the model are to:

1) Reduce the complexity and execution time of the calculation. In commercial flow simulation models, robustness and computational speed are important factors, and simplifications will generally benefit both.
2) Simplifications can reduce the number of model coefficients. In our specific case, if we can reduce droplet size distribution to a single representative droplet size, we circumvent the need for extra parameters describing the distribution function.

As we have alluded to several times at this point, we would like to replace the droplet size distribution with a single droplet size. A

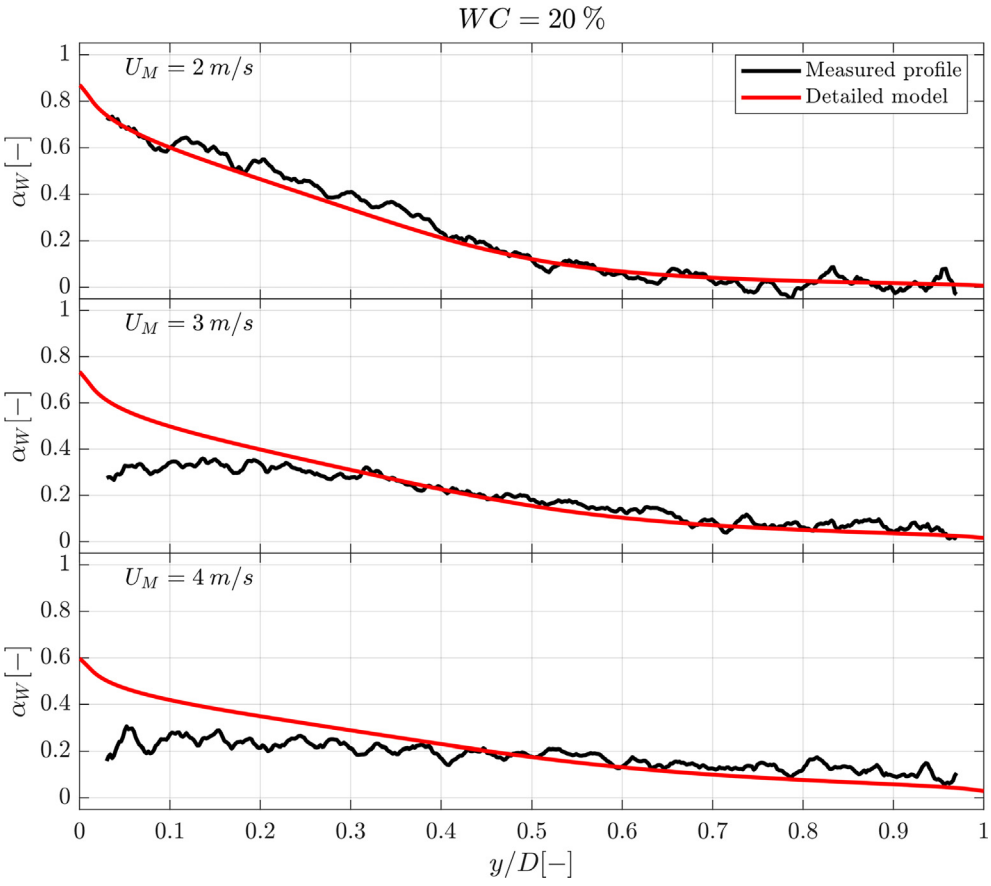

Fig. 6. Measured and predicted volumetric water concentration profiles for WC = 20 % and U_M = 2, 3 and 4 m/s. y/D = 0 represents the pipe bottom, and y/D = 1 represents the top of the pipe. The predictions are based on the detailed model described above, which uses the measured droplet size distributions and the Reichardt model for the diffusivity profile (Reichhardt, 1951).

common approach for simplifying droplet size distributions is to use the Sauter mean droplet diameter d_{32}, which is defined by Eq. (4). When calculating the Sauter mean values, we included droplet size measurements at all the vertical positions in the pipe.

By replacing the measured droplet size distributions with the associated Sauter mean values, we obtained concentration profiles that were very close to those from the full model. Fig. 7 shows results obtained with and without this simplification, along with the experimental data for the two experiments shown in the previous section. It seems clear from these examples that the Sauter mean droplet size yields a good representation of the droplet size distributions for the present model. Although we only show three examples here, we tested this on many other experiments with the same conclusion.

The reason for the success of the Sauter mean droplet size is not obvious, but in the following paragraphs we will attempt to derive a qualitative explanation:

The contribution of each droplet size bin in the droplet size distribution to the total concentration profile equals$p_i C_i$, where p_i is the volumetric fraction associated with droplet size bin i. The parameter p_i is thus defined as the volume weighted droplet size bin:

$$p_i = \frac{d_i^3 P_i}{\sum_i d_i^3 P_i} = \frac{d_i^3 P_i}{\left\langle d^3 \right\rangle} \tag{27}$$

where P_i (capital P) represents the raw droplet size distribution. The droplet Reynolds numbers in the present experiments are well above unity, and the associated relationship between the droplet size and the settling velocity is then approximately linear:

$$U_{T0} = \frac{4\Delta\rho g d}{3\rho_O C_D} = k \cdot d \tag{28}$$

Here, given the relevant Reynolds numbers, k can be assumed to be approximately independent of the droplet diameter d. The droplet size distributions for each droplet size bin can (by assuming a constant diffusivity and ignoring hindrance and turbulence effects) be approximated by:

$$C_i(y) \approx C_0 p_i \exp\left(-\frac{U_{T0,i} y}{\varepsilon_P}\right) \tag{29}$$

If we further assume channel flow instead of pipe flow, we may estimate the total droplet concentration C_{tot} by integrating the above equation over the height of the channel/pipe, yielding:

$$C_{tot} \approx \sum_i \frac{\varepsilon_P C_0 p_i}{D U_T}\left[1 - \exp\left(-\frac{U_{T0,i} D}{\varepsilon_P}\right)\right] \tag{30}$$

By including only the leading term, we get:

$$C_{tot} \sim \sum_i \frac{\varepsilon_P C_0 p_i}{D U_T} \tag{31}$$

Finally, by substituting Eqs. (27) and (28) into (31), we obtain:

$$C_{tot} \sim \sum_i \frac{\varepsilon_P C_0}{D \cdot k \cdot d_i} \frac{d_i^3 P_i}{\left\langle d^3 \right\rangle} = \sum_i \frac{\varepsilon_P C_0}{D \cdot k} \frac{d_i^2 P_i}{\left\langle d^3 \right\rangle} = \frac{\varepsilon_P C_0}{D \cdot k} \frac{\left\langle d^2 \right\rangle}{\left\langle d^3 \right\rangle}$$
$$= \frac{\varepsilon_P C_0}{D \cdot k \cdot d_{32}} = \frac{\varepsilon_P C_0}{D \cdot U_{T0}(d = d_{32})} \tag{32}$$

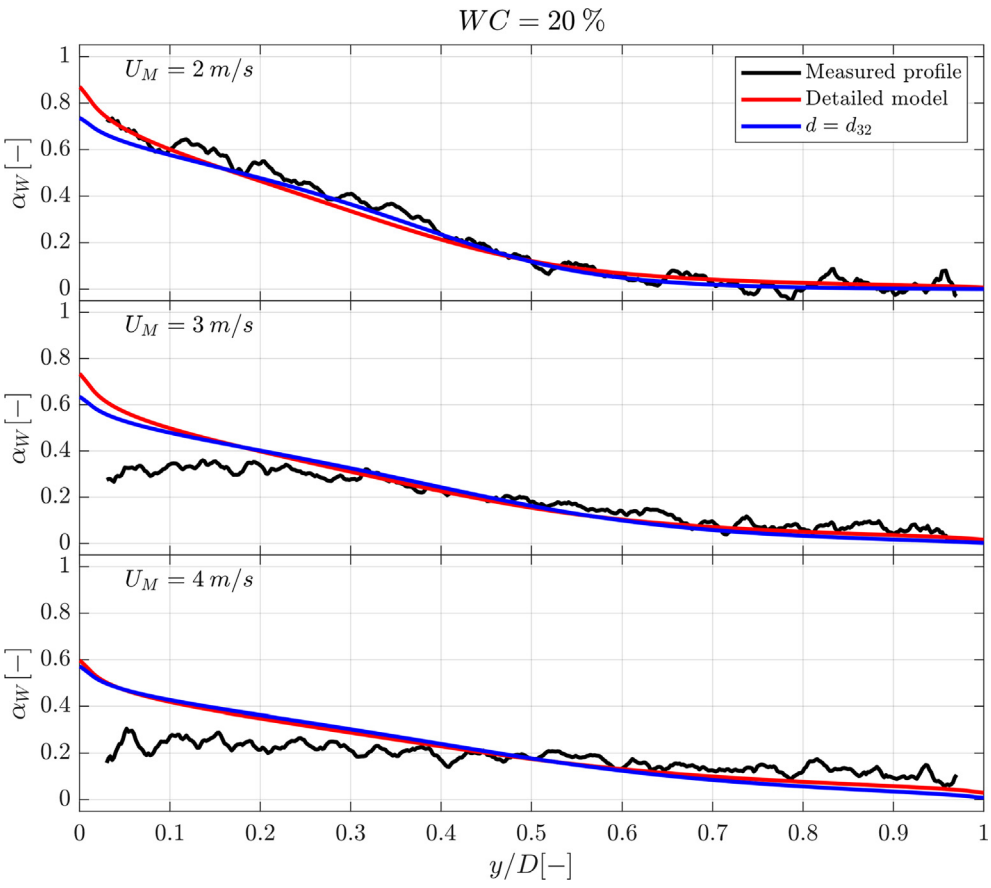

Fig. 7. Measured and predicted volumetric water concentration profiles for WC = 20 % and U_M = 2, 3 and 4 m/s. y/D = 0 represents the pipe bottom, and y/D = 1 represents the top of the pipe. The predictions are based on the gravity/diffusion model using the measured Sauter mean droplet diameters instead of the respective droplet size distributions.

Consequently, given these rough approximations, we find that the total volume fraction of droplets (given some boundary concentration C_0) can be roughly estimated by replacing the droplet size distribution by the Sauter mean diameter in the settling velocity calculation. This would then arguably suggest that the concentration profile obtained with the Sauter mean diameter might also be in reasonable agreement with the exact solution.

We must point out that since the above derivation includes several loose approximations, it is difficult to evaluate the adequacy of the simplification based on the derivation alone. However, as shown in Fig. 7, the model predictions appear to support the notion that the Sauter mean diameter is indeed a good approximation of the droplet size distribution.

The other simplification that we investigated was to replace the eddy diffusivity profile given by Eq. (12) by a constant diffusivity. This simplification does not provide much benefit in terms of computational speed or complexity, but it can at least tell us something about the importance (or lack thereof) of the details of the diffusivity model. In Fig. 8 we have plotted the results obtained using the Reichardt diffusivity model (Eq. (12)) and using a constant dimensionless diffusivity of 0.07. The value of 0.07 was selected because this was approximately the mean value in the core region in the Reichardt diffusivity model (see Fig. 5) and should thus be a reasonable approximation. Indeed, in a pipe geometry, the modelling of the core region is in a sense more important than the near-wall regions because that is where most of the flow area is. Specifically, the treatment of the near-wall region does not have much impact on the resulting concentration profile elsewhere. This is reflected in Fig. 8, where we observe that aside from some minor artifacts at the pipe bottom, the two approaches give virtually the same profiles. We thus conclude that we can replace the Reichardt diffusivity model with a constant dimensionless diffusivity of 0.07 without any significant loss of accuracy. It may also be argued that near-wall effects such as lift forces (Saffman, 1965), particle–wall collisions (Sommerfeld, 1992; Tian, 2006), and granular pressure (B. G. M. v. Wachem, J. C. Schouten, C. M. v. d. Bleek, R. Krishna and J. L. Sinclair, , 2001; Gidaspow, 1994; Laux, 1998) would in practice prevent the effective diffusivity from becoming very low, hence the constant-diffusivity approximation might therefore be adequate.

3.6. Accounting for turbulence in the drift velocity model

In the described model we have computed the drag coefficient C_D using Eq. (17), calculating the associated Reynolds numbers based on the settling velocity U_T. One effect that we have not yet accounted for is that the motion of the droplets is continuously disturbed by the turbulent velocity fluctuations of the surrounding fluid, so that the instantaneous droplet-fluid slip will in practice fluctuate around the mean value. For sufficiently small droplet Reynolds numbers Re_D, only the first term in the drag coefficient expression (17) is important, and the prevailing drag force would then be linear in the droplet-fluid slip velocity, in which case the fluctuations would cancel out on average because the drag force fluctuations would be symmetric. However, in our case, the droplet Reynolds numbers are in the range 4–20, and the second term in Eq. (17) is significant. The consequence is that the drag force is non-linear in the droplet-fluid slip velocity, and that the resulting drag force fluctuations are not symmetric. Specifically, an increase in the local droplet-fluid slip velocity will lead to a larger change in

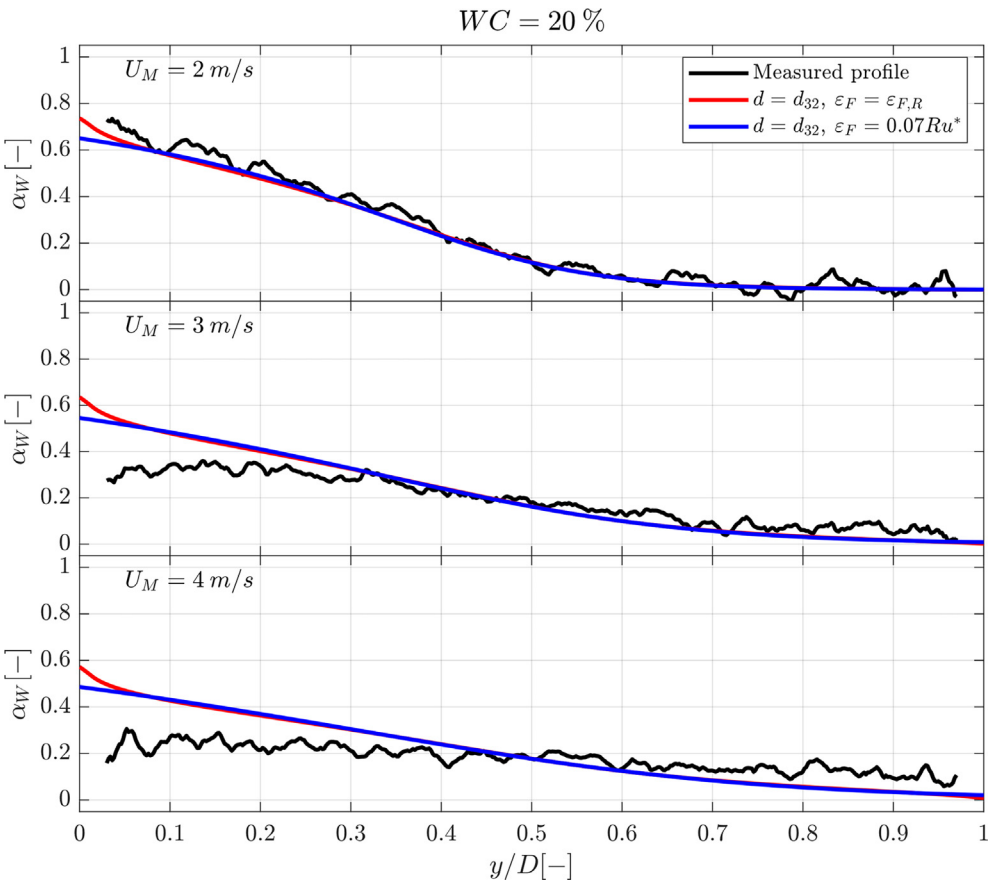

Fig. 8. Measured and predicted volumetric water concentration profiles for WC = 20 % and U_M = 2, 3 and 4 m/s. y/D = 0 represents the pipe bottom, and y/D = 1 represents the top of the pipe. The predictions are based on the gravity/diffusion model using the measured Sauter mean droplet diameters and assuming a constant dimensionless diffusivity of 0.07.

the drag force compared to a corresponding reduction in the droplet-fluid slip velocity.

The instantaneous vertical drag force F_D on the droplets is given by:

$$F_D = \frac{1}{2}\rho_F C_D A_D |u_D - u_F|(u_D - u_F) \tag{33}$$

Where A_D is the droplet cross section area, u_D and u_F are the instantaneous vertical droplet- and fluid velocities. Substituting Eqs. (17) and (18), into Eq. (33), and replacing the terminal velocity U_{T0} with $|u_D\text{-}u_F|$ in the Reynolds number expression gives:

$$F_D = \frac{12\mu_F A_D}{d_D}\left(1 + 0.15\left(\frac{\rho_F d_D |u_D - u_F|}{\mu_F}\right)^{0.687}\right)(u_D - u_F) \tag{34}$$

The average drag force $\langle F_D \rangle$ is then:

$$\langle F_D \rangle = \frac{12\mu_F A_D}{d_D}\left(\langle u_D - u_F \rangle + 0.15\left(\frac{\rho_F d_D}{\mu_F}\right)^{0.687}\left\langle |u_D - u_F|^{0.687}(u_D - u_F)\right\rangle\right) \tag{35}$$

As explained above, the expression $\langle u_D - u_F \rangle$ simply equals the average drift velocity U_{T0}, but the expression $\left\langle |u_D - u_F|^{0.687}(u_D - u_F)\right\rangle$ requires some attention. The first step towards evaluating this expression is to examine the averaged squared slip velocity:

$$\langle (u_D - u_F)^2 \rangle = \langle u_D^2 \rangle + \langle u_F^2 \rangle - 2\langle u_D u_F \rangle \tag{36}$$

We now split the instantaneous droplet velocity into an average value U_{T0}, and a fluctuating component u' with a mean value of zero:

$$u_D = U_{T0} + u' \tag{37}$$

We note that the instantaneous vertical fluid velocity u_F has a mean value of zero, so there is no need to decompose u_F. We then obtain:

$$\begin{aligned}\langle (u_D - u_F)^2 \rangle &= \langle (U_{T0} + u\prime - u_F)^2 \rangle \\ &= U_{T0}^2 + \langle u\prime^2 \rangle + \langle u_F^2 \rangle\text{`} - 2\langle u\prime u_F \rangle\end{aligned} \tag{38}$$

In the last transition, we exploited the fact that $\langle u' \rangle = \langle u_F \rangle = 0$. We now apply what Skartlien (Skartlien, 2009) refers to as the "locally homogeneous approximation", meaning that we treat the turbulence as if it were locally homogeneous. According to Skartlien (Skartlien, 2009) and Pourahmadi (Pourahmadi, 1982), this approximation leads to:

$$\langle u'^2 \rangle \approx \frac{\langle u_F^2 \rangle}{1 + St} \tag{39}$$

$$\langle u' u_F \rangle \approx \frac{\langle u_F^2 \rangle}{1 + St} \tag{40}$$

The square of the fluid velocity fluctuations $\langle u_F^2 \rangle$ can be approximated by (Hay et al., 1996; Pan and Hanratty, 2002):

$$\langle u_F^2 \rangle = (0.9 \cdot U^*)^2 \tag{41}$$

where U^* is the average friction velocity, which we calculate from the measured frictional pressure drop, see Eq. (9). The Stokes number St is defined as the ratio of the droplet relaxation time scale τ_D and the integral turbulence time scale τ_F. We define the droplet relaxation time τ_D as (Lee et al., 1989; Pan and Hanratty, 2002):

$$\tau_D = \frac{\rho_D U_{T0}}{\Delta\rho \cdot g_y} \tag{42}$$

The integral turbulence time scale τ_F can be calculated from the eddy diffusivity ε_F (Skartlien, 2009):

$$\tau_F = \frac{\varepsilon_F}{\langle u_F^2 \rangle} \tag{43}$$

Substituting Eqs. (39) and (40) into (38) leads to the following expression for the average squared slip velocity:

$$\left\langle (u_D - u_F)^2 \right\rangle = U_{T0}^2 + \langle u_F^2 \rangle \frac{St}{1 + St} \tag{44}$$

From this expression we observe that the slip velocity can effectively be represented by the sum of a mean component of magnitude U_{T0}, and a fluctuating component with a mean squared value equal to $\langle u_F^2 \rangle St/(1 + St)$. Consequently, assuming that the velocity fluctuations u_F are normally distributed, the slip velocity distribution can be represented by a Gaussian distribution centred around U_{T0}, with a variance of $\langle u_F^2 \rangle St/(1 + St)$. This insight allows us to evaluate the expression $\left\langle |u_D - u_F|^{0.687}(u_D - u_F)\right\rangle$ by numerically integrating the associated Gauss distribution:

$$\left\langle |u_D - u_F|^{0.687}(u_D - u_F)\right\rangle = \frac{1}{\sqrt{2\pi\sigma^2}}\int_{-\infty}^{\infty} x \cdot |x^{0.687}| \exp\left(\frac{-(x - U_{T0})^2}{2\sigma^2}\right) \cdot dx \tag{45}$$

where we have defined σ^2 as:

$$\sigma^2 = \langle u_F^2 \rangle \frac{St}{1 + St} = (0.9 \cdot U^*)^2 \frac{St}{1 + St} \tag{46}$$

The expression for calculating $U_{T0} = \langle u_D - u_F \rangle$ can be obtained by setting the drag force (Eq. (35)) equal to the sum of the gravity/buoyancy forces:

$$\begin{aligned}&\frac{12\mu_F}{d_D}\frac{\pi d_D^2}{4}\left(\langle u_D - u_F \rangle + 0.15\left(\frac{\rho_F d_D}{\mu_F}\right)^{0.687}\left\langle |u_D - u_F|^{0.687}(u_D - u_F)\right\rangle\right) \\ &= \frac{\pi d_D^3(\rho_D - \rho_F)g_y}{6}\end{aligned} \tag{47}$$

Some minor re-arrangement yields the following expression:

$$\begin{aligned}&\langle u_D - u_F \rangle + 0.15\left(\frac{\rho_F d_D}{\mu_F}\right)^{0.687}\left\langle |u_D - u_F|^{0.687}(u_D - u_F)\right\rangle \\ &= \frac{g_y d_D^2(\rho_D - \rho_F)}{18\mu_F}\end{aligned} \tag{48}$$

Using the fact that $\langle u_D - u_F \rangle = U_{T0}$ and Eq. (45), we get:

$$\begin{aligned}&U_{T0} + 0.15\left(\frac{\rho_F d_D}{\mu_F}\right)^{0.687} \cdot \frac{1}{\sqrt{2\pi\sigma^2}}\int_{-\infty}^{\infty} x \cdot |x^{0.687}| \exp\left(\frac{-(x - U_{T0})^2}{2\sigma^2}\right) \cdot dx \\ &= \frac{g_y d_D^2(\rho_D - \rho_F)}{18\mu_F}\end{aligned} \tag{49}$$

This expression can be rewritten as:

$$U_{T0} = \frac{U_{Stokes}}{1 + \frac{0.15}{U_{T0}}\left(\frac{\rho_F d_D}{\mu_F}\right)^{0.687}\frac{1}{\sqrt{2\pi\sigma^2}}\int_{-\infty}^{\infty} x \cdot |x^{0.687}| \exp\left(\frac{-(x - U_{T0})^2}{2\sigma^2}\right) \cdot dx} \tag{50}$$

where we have defined U_{Stokes} as:

$$U_{Stokes} = \frac{g \cdot d_D^2(\rho_D - \rho_F)}{18\mu_F} \tag{51}$$

In our model, Eq. (50) was solved iteratively using simple successive substitution.

4. Results and discussion

Figs. 9-13 show the prevailing results for all the experiments, where we have included predictions both with and without the turbulence correction on the drag coefficient, with solid and dashed lines, respectively. We observe that the turbulence correction significantly improves the agreement with the data for $U_M \geq 3$ m/s. Meanwhile, for U_M = 2 m/s, the predictions are arguably more accurate without this correction. Nevertheless, it would be difficult to argue in favour of omitting this correction, and we thus suspect that the deviations that we observe for the experiments at U_M = 2 m/s come from either some of the approximations/assumptions made in the modelling, or from weaknesses in some of the sub-models.

The deviations observed for U_M = 2 m/s are perhaps not very large, but they are consistent in that the predictions always show too homogeneous profiles. At this flow rate, we observed that the droplet sizes were more heterogeneously distributed than at higher rates (see Fig. 3), with larger droplets at the bottom of the pipe than elsewhere. To check whether this might be the source of the discrepancies, we re-calculated the concentration profiles using the droplet sizes measured at the bottom of the pipe. This did however not change the concentration profiles very much, so the heterogeneous droplet size distributions do not appear to be the reason for the deviations at U_M = 2 m/s.

One might suspect that the discrepancies observed for U_M = 2 m/s could be related to the fact that the concentrations at the bottom of the pipe are typically higher compared to cases with higher liquid rates. However, we observe in Figs. 9-13 that the magnitude of the discrepancies does not appear to depend appreciably on the water cut, suggesting that the discrepancies are not associated with high droplet concentrations. For instance, at U_M = 2 m/s and WC = 5 %, the maximum concentration is about 20 %, which is smaller than many of the concentrations obtained at higher liquid rates.

We should point out that there are several physical effects that we have not included in our model. Some of these omitted effects are related to phenomena that occur in the near-wall regions. Among these near-wall effects, we can mention lift forces (Saffman, 1965), particle–wall collisions (Sommerfeld, 1992; Tian, 2006); turbophoresis (Reeks, 1983), and granular pressure (B. G. M. v. Wachem, J. C. Schouten, C. M. v. d. Bleek, R. Krishna and J. L. Sinclair, , 2001; Gidaspow, 1994; Laux, 1998). However, based on the results shown in Section 3.5, were we showed that the results were rather insensitive to the modelling of the near-wall regions, we do not believe that the inclusion of these effects would improve the predictions.

Another effect that we have neglected is added mass (Stokes, 1851), where the effective inertial mass of accelerating droplets is enhanced by the fact that the surrounding fluid must also be accelerated. A simple model for this effect was proposed by van Wijngaarden (van Wijngaarden, 1976), where the added mass m_A of a particle with volume V_D suspended in a fluid with density ρ_F is given by:

$$m_A = \frac{1}{2}\rho_F V_D(1 + 2.78 \cdot C) \tag{52}$$

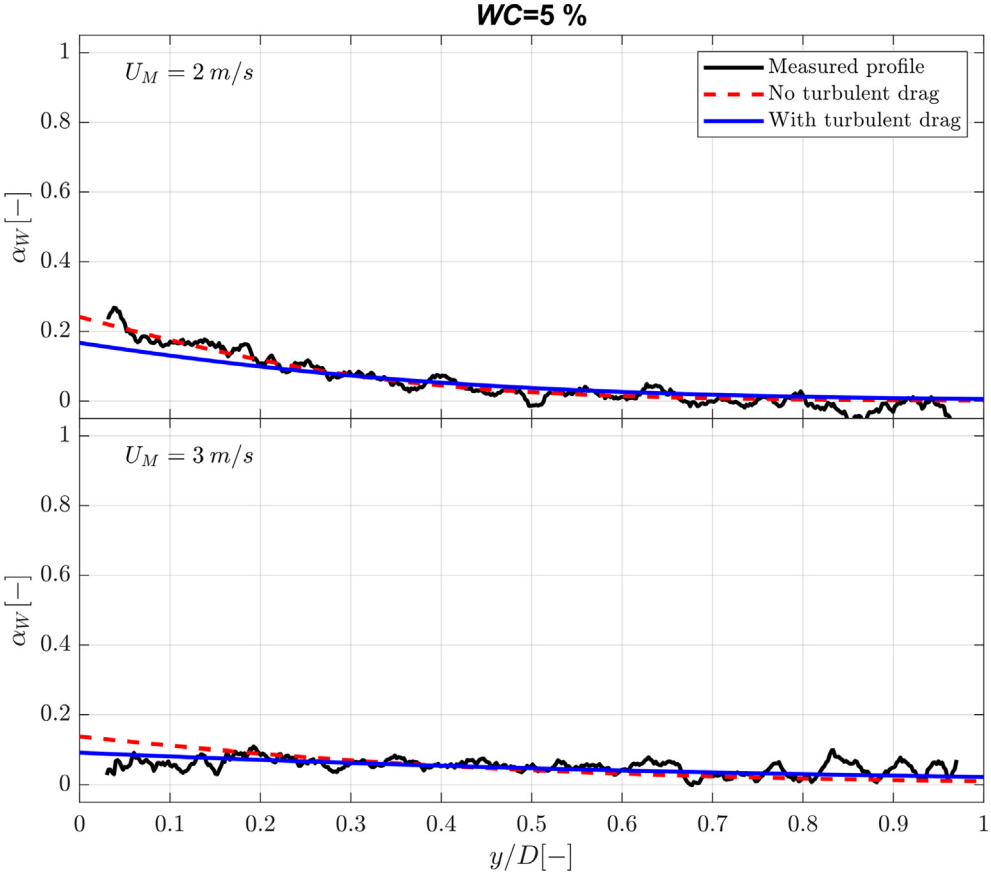

Fig. 9. Measured and predicted volumetric water concentration profiles for WC = 5 %. y/D = 0 represents the pipe bottom, and y/D = 1 represents the top of the pipe. The black lines represent the measurements, the red dashed lines represent the model without accounting for the impact of turbulence on the drift velocity, and the blue solid lines represent the model with this effect included. (For interpretation of the references to colour in this figure legend, the reader is referred to the web version of this article.)

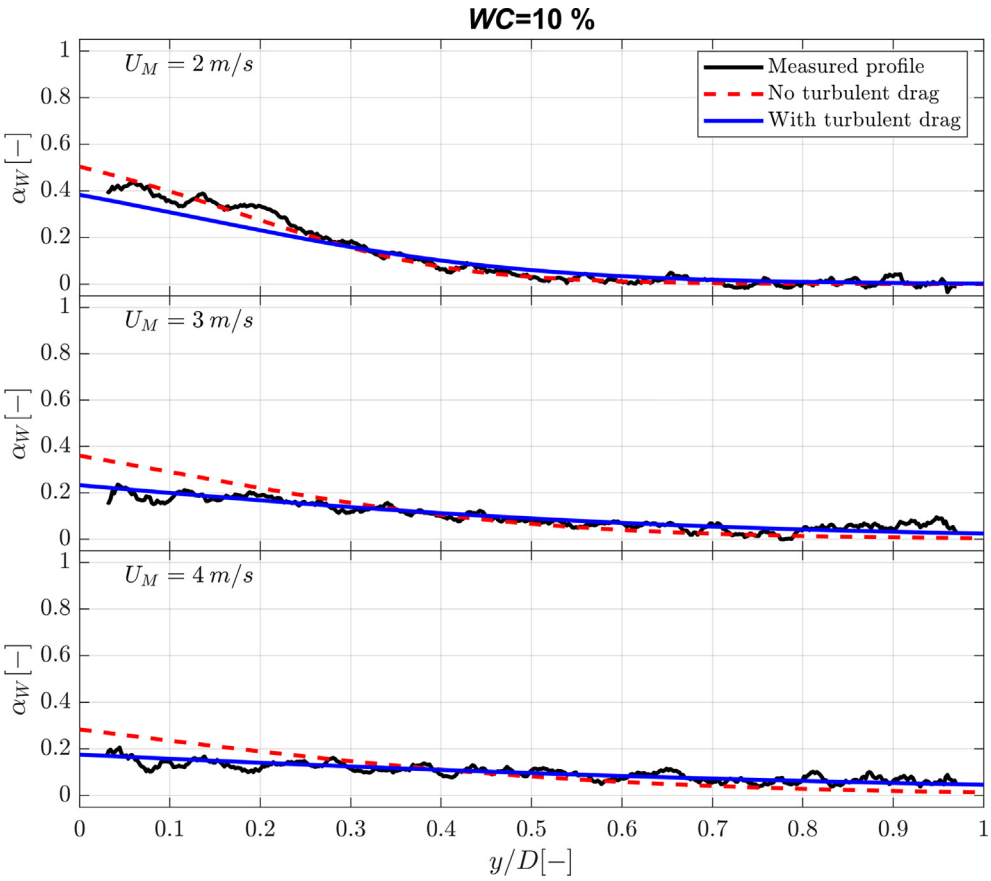

Fig. 10. Measured and predicted volumetric water concentration profiles for WC = 10 %. y/D = 0 represents the pipe bottom, and y/D = 1 represents the top of the pipe. The black lines represent the measurements, the red dashed lines represent the model without accounting for the impact of turbulence on the drift velocity, and the blue solid lines represent the model with this effect included. (For interpretation of the references to colour in this figure legend, the reader is referred to the web version of this article.)

where C is the particle concentration. The added mass affects how the droplets respond to the turbulent fluctuations, effectively yielding an increase in the droplet Stokes number of magnitude:

$$St \rightarrow St \cdot \left(1 + \frac{\rho_F}{2\rho_D}(1 + 2.78 \cdot C)\right) \tag{53}$$

However, testing revealed that introducing added mass did not have a significant effect on the results.

One possible weakness in our model is that we have used the empirical hindrance model by Richardson & Zaki (Richardson and Zaki, 1954), which was developed using data from fluidised beds. The physical interpretation of this model is unclear, so although it has been shown to be accurate for fluidised beds, it is not obvious that it should work equally well for the turbulent flowing systems examined in this paper. Also, we have opted to super-impose the hindrance effect on top if the effect of turbulence, implicitly assuming that the two effects are independent, which might not be the case.

Another possible weakness may come from the various approximations and assumptions related to the calculation of the slip velocity distribution, which depends critically on the Stokes number St, see Eq. (44). It seems clear that Eq. (44) behaves as expected in the low- and high Stokes number limits. At low Stokes numbers, Eq. (44) reduces to $\left\langle (u_D - u_F)^2 \right\rangle = U_{T0}^2$, meaning that the droplets behave as inert tracer particles that respond instantaneously to the turbulent fluctuations. At high Stokes numbers, Eq. (44) reduces to $\left\langle (u_D - u_F)^2 \right\rangle = U_{T0}^2 + \langle u_F^2 \rangle$, meaning that the droplets are so heavy that they do not respond to the turbulent fluctuations at all. However, the Stokes numbers encountered in the present experiments are in the range 0.3–0.9, putting them squarely in the "intermediate" and thus most challenging range, where the model is most likely to be inaccurate. Consequently, it is possible that the discrepancies could at least partially be attributed to uncertainties associated with Eq. (44).

Finally, it is worth restating that we have assumed that the turbulence is unaffected by the presence of droplets, which is arguably questionable, especially for the cases with the highest volumetric droplet concentrations. Specifically, particles can increase the dissipation of turbulent kinetic energy (Yuan and Michaelides, 1992), leading to a reduction in diffusivity and effective form drag. Indeed, according to Gore & Crowe (Gore and Crowe, 1989), particles with sizes less than 10 % of the characteristic length scale of the most energetic eddies tend to reduce the

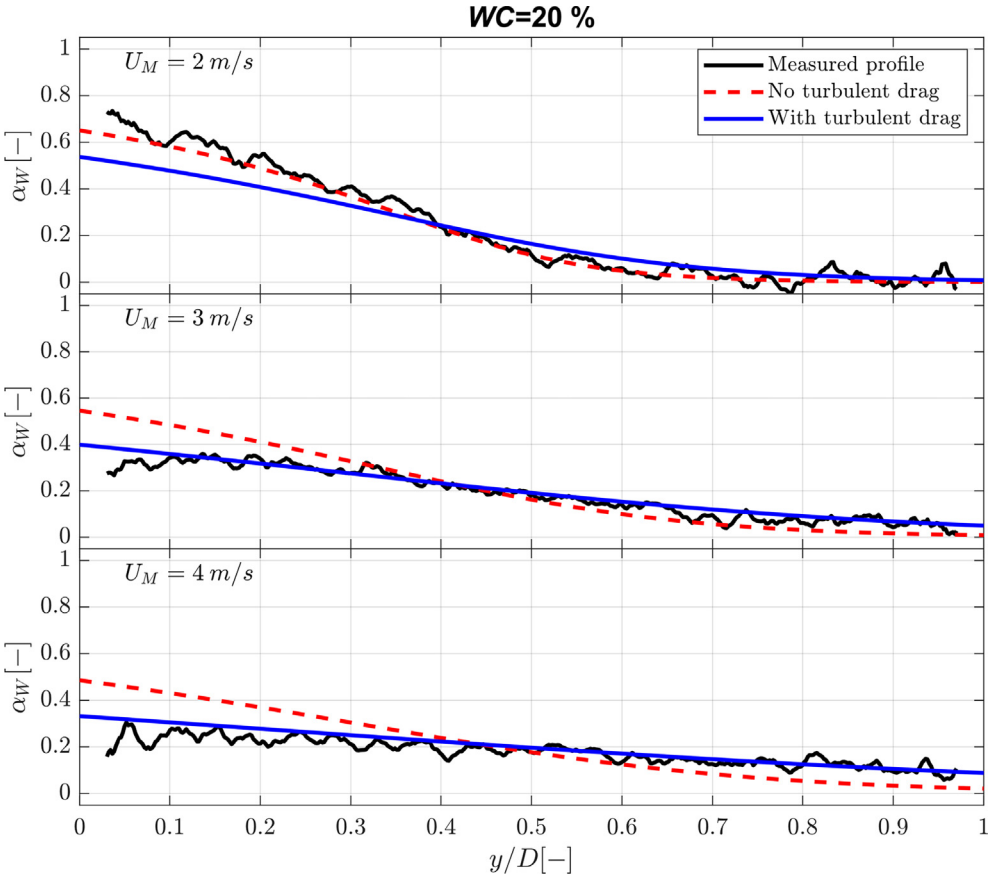

Fig. 11. Measured and predicted volumetric water concentration profiles for WC = 20 %. y/D = 0 represents the pipe bottom, and y/D = 1 represents the top of the pipe. The black lines represent the measurements, the red dashed lines represent the model without accounting for the impact of turbulence on the drift velocity, and the blue solid lines represent the model with this effect included. (For interpretation of the references to colour in this figure legend, the reader is referred to the web version of this article.)

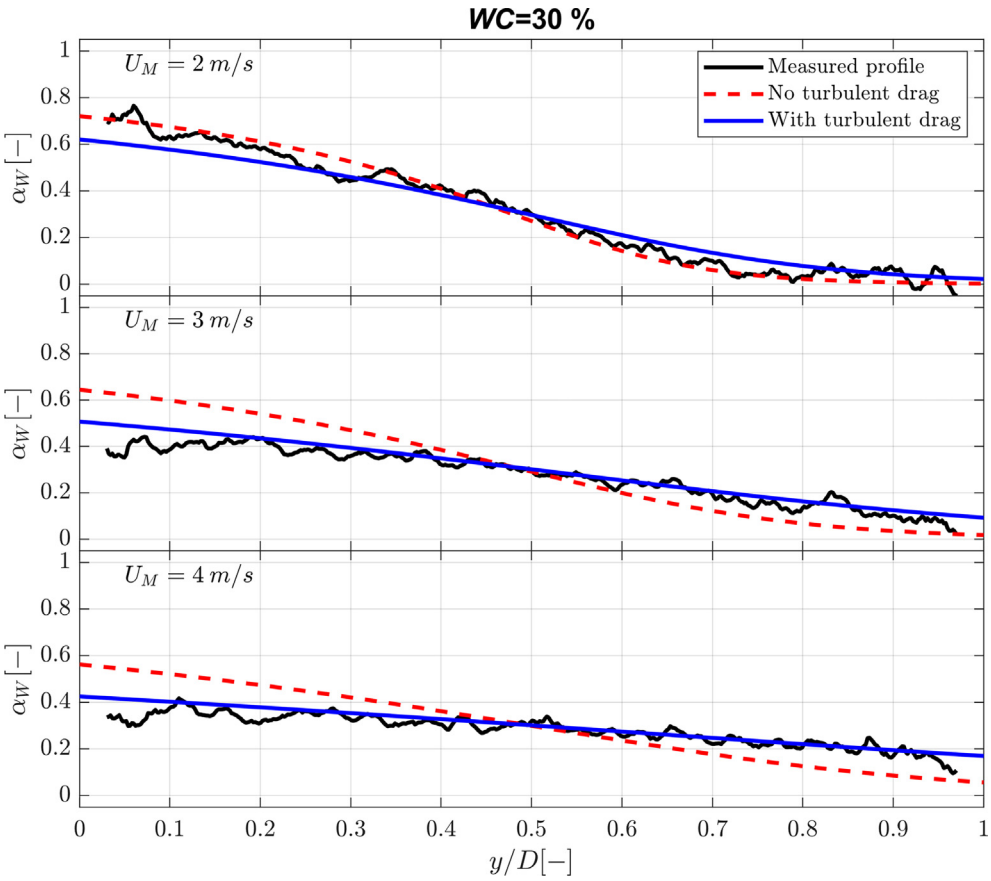

Fig. 12. Measured and predicted volumetric water concentration profiles for WC = 30 %. y/D = 0 represents the pipe bottom, and y/D = 1 represents the top of the pipe. The black lines represent the measurements, the red dashed lines represent the model without accounting for the impact of turbulence on the drift velocity, and the blue solid lines represent the model with this effect included. (For interpretation of the references to colour in this figure legend, the reader is referred to the web version of this article.)

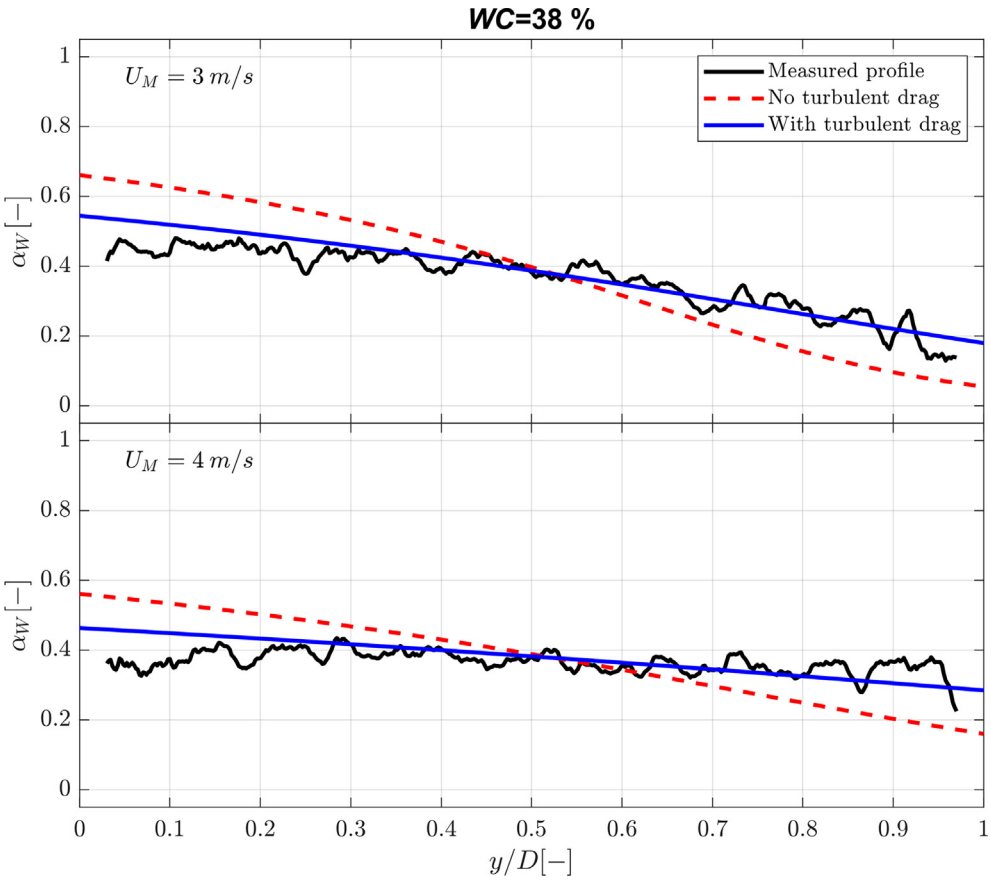

Fig. 13. Measured and predicted volumetric water concentration profiles for WC = 38 %. *y/D* = 0 represents the pipe bottom, and *y/D* = 1 represents the top of the pipe. The black lines represent the measurements, the red dashed lines represent the model without accounting for the impact of turbulence on the drift velocity, and the blue solid lines represent the model with this effect included. (For interpretation of the references to colour in this figure legend, the reader is referred to the web version of this article.)

turbulence intensity. We suspect that this might be one of the main causes for the discrepancies between the model and the data for the lowest flow rate (2 m/s).

5. Conclusions

In this work we implemented a gravity-diffusion model for predicting water concentration profiles in dispersed oil-continuous oil–water flows and compared the predictions to the experiments reported by Gonzales et al. (Gonzalez et al., 2022).

The motivation for this work is that there is a need for simple but effective computational models for oil/water flows. Specifically, when oil/water is transported over long distances, the model execution times of full 3D models can be prohibitive. A more pragmatic approach is then called for, and the model outlined in this paper represents such an approach.

The turbulent diffusion was modelled using a single-phase closure law developed by Reichardt (Reichhardt, 1951), and the model for gravitational drift was based on the drag model by Clift et al. (Clift and Weber, 1988), combined with the hindrance model by Richardson & Zaki (Richardson and Zaki, 1954).

The model did not include a closure law for the droplet sizes, instead the measured droplet sizes were used. This has not been possible before since no previous experimental oil/water studies have included both phase fraction profiles and droplets sizes. The benefit of this was that we could focus on the closure laws related to turbulent diffusion and gravitational drift. Previous modelling efforts have been hampered by the lack of droplet size measurements and have been forced to deploy closure laws with unknown accuracy for the droplet size. This has apparently led to a wide range of models for turbulent diffusion in the literature, some of which are quite far from the values expected for single phase flow (Amundsen, 2011; Paolinelli, 2020). Meanwhile, in this study, a simple single phase closure law for turbulent diffusion was found to be generally adequate.

The results showed that including the effect of turbulence on the drag force is important, where the turbulent fluctuations cause an increase in the average drag because of the non-linearity of the drag law. Specifically, omitting this effect caused significant deviations at the highest flow rates (*UM* = 3–4 m/s). At the lowest flow rate (*UM* = 2 m/s), the model was found to predict profiles that were slightly more homogenous than the data, suggesting that the model has some weaknesses for moderate rates. We suspect that those deviations might be caused by turbulence modulation induced by the droplet field.

We also concluded that the following model simplifications could be introduced without changing the results significantly:

1) The droplet size distributions could be replaced by the Sauter mean droplet size. This simplification substantially improved the computational speed and robustness of the model.
2) The Reichardt diffusivity profile model could be replaced by a uniform diffusivity model with a dimensionless diffusivity of 0.07.

CRediT authorship contribution statement

Jørn Kjølaas: Conceptualization, Validation, Methodology, Software, Investigation, Data curation, Writing – original draft, Visual-

ization, Supervision. **Heiner Schümann:** Data curation, Investigation, Writing – review & editing, Project administration, Funding acquisition. **Diana Gonzalez:** Data curation, Investigation. **Stein Tore Johansen:** Conceptualization, Methodology, Supervision, Writing – review & editing.

Data availability

Data will be made available on request.

Declaration of Competing Interest

The authors declare that they have no known competing financial interests or personal relationships that could have appeared to influence the work reported in this paper.

Acknowledgements

The work has been conducted as part of NexFlow, an industry knowledge-building project (NFR project number 295035) financed by TotalEnergies EP Norge AS and the Research Council of Norway.

References

Amundsen, L., 2011. An experimental study of oil-water flow in horizontal and inclined pipes. Norges teknisk-naturvitenskapelige universitet, Trondheim.
Batchelor, G.K., 1966. The Motion of Small Particles in Turbulent Flow. In: Second Australasian Conference on Hydraulics and Fluid Mechanics, The University of Auckland, New Zealand.
Berrio, J.C., Pinilla, A., Ratkovich, N., 2021. CFD study of oil-water segregated and dispersed flow coalescence in horizontal pipes. Chem. Eng. Commun. 208 (12), 1695–1710.
Biberg, D., 2005. Mathematical Models for Two-phase Stratified Pipe Flow. University of Oslo. PhD Thesis.
Binder, J.L., Hanratty, T.J., 1992. Use of lagrangian methods to describe drop deposition and distribution in horizontal gas-liquid annular flows. Int. J. Multiphase Flow 18 (6), 803–820.
Brauner, N., 2003. Liquid-Liquid Two-Phase Flow Systems. In: Modelling and Experimentation in Two-Phase Flow, vol. 450, Vienna, Springer Vienna, pp. 221-279.
Chen, C., 1990. Unified theory on power laws for flow resistance. J. Hydraulic Eng., ASCE 117 (3), 371–389.
Clift, R., Weber, M.E., 1988. Bubbles, drops and particles. Academic Press, London.
COMSOL, 2019. Multiphysics 5.3, COMSOL.
Elseth, G., 2001. An Experimental Study of Oil/Water Flow in Horizontal Pipes. Norwegian University of Science and Technology (NTNU), Telemark.
Fluent User's Guide Release 14, 2011. Washington, PA, USA: Ansys Inc.
Gidaspow, D., 1994. Multiphase Flow and Fluidization, Continuum and Kinetic Theory Descriptions. Academic Press.
Gonzalez, D., Schümann, H., Kjølaas, J., 2022. "Pipe flow experiments of unstable oil-water dispersions with three different oil viscosities: flow pattern, pressure drop and droplet size measurements. J. Petrol. Sci. Eng.
Gore, R.A., Crowe, C.T., 1989. Effect of particle size on modulating turbulent intensity. Int. J. Multiph. Flow 15 (2), 279–285.
Gudmundsson, J.S., Bott, T.R., 1977. Particla diffusivity in turbulent pipe flow. J. Aerosol Sci. 8, 317–319.
Guha, A., 2008. Transport and deposition of particles in turbulent and laminar flow. Annu. Rev. Fluid Mech. 40 (1), 311–341.
Haider, A., Levenspiel, O., 1989. Coefficient and Terminal Velocity of Spherical and Nonspherical Particles. Powder Technol. 58 (1), 63–70.
Hay, K.J., Liu, Z.-C., Hanratty, T.J., 1996. Relation of deposition to drop size when the rate law is nonlinear. Int. J. Multiphase Flow 22 (5), 829–848.
Hinze, J.O., 1955. "Fundamentals of the hydrodynamic mechanism of splitting in dispersion process. AIChE 289 (1).
Hinze, J.O., 1972. Turbulent fluid and particle interaction. In: Proc. Int. Symposium Two-Phase Syst.. Elsevier, pp. 433–452.
Hunt, J.N., 1954. The turbulent transport of sus ended sediment in open channels. Roy. Soc. London Proc., Ser. A 224 (1158), 322–335.
Johansen, S.T., 1991. The deposition of particles on vertical walls. Int. J. Multiphase Flow 17 (3), 355–376.
Joseph, D.D., Bai, R., Chen, K.P., Renardy, Y.Y., 1997. Core-annular flows. Annu. Rev. Fluid Mech. 29 (1), 65–90.
Karbelas, A.J., 1977. Vertical distribution of dilute suspensions in turbulent pipe flow. AIChE J. 23 (4), 426–434.
Kumara, W.A.S., Halvorsen, B.M., Melaaen, M.C., 2009. Pressure drop, flow pattern and local water volume fraction measurements of oil–water flow in pipes. Meas. Sci. Technol. 20 (11).
Laux, H., 1998. Modeling of Dilute and Dense Dispersed Fluid-Particle Two-Phase Flow. Norwegian University of Science and Technology, Trondheim, Norway. PhD dissertation.
Lee, M.M., Hanratty, T.J., Adrian, R.J., 1989. The interpretation of droplet deposition measurements with a diffusion model. Int. J. Multiphase Flow 15 (3), 459–469.
Liu, B.Y.H., Ilori, T.A., 1974. Aerosol deposition in turbulent pipe flow. Environ. Sci. Technol. 8 (4), 351–356.
Nikuradse, J., 1933. Strömungsgesetze in rauhen Rohren. VDI-Verlag.
Pal, R., Rhodes, E., 1989. Viscosity/Concentration Relationships for Emulsions. J. Rheol. 33 (7), 1021–1045.
Pan, L., Hanratty, T.J., 2002. Correlation of entrainment for annular flow in horizontal pipes. Int. J. Multiph. Flow 28 (3), 385–408.
Paolinelli, L.D., 2020. A comprehensive model for stability of dispersed oil-water flow in horizontal and inclined pipes. Chem. Eng. Sci. 211, 115325.
Picart, A., Berlemont, A., Gouesbet, G., 1986. Modelling and predicting turbulence fields and the dispersion of discrete particles transported by turbulent flows. Int. J. Mult. Flow 12 (2), 237–261.
Pourahmadi, F., 1982. Turbulence modeling of single and two phase curved channel flows, University of California, Berkeley ProQuest Dissertations Publishing.
Pouraria, H., Park, K.-H., Seo, Y., 2021. Numerical modelling of dispersedwater in oil lows using eulerian-eulerian approach and population balance model. Processes 9.
Reeks, M.W., 1977. On the dispersion of small particles suspended in an isotropic turbulent fluid. J. Fluid Mech. 83 (3), 529–546.
Reeks, M.W., 1983. The transport of discrete particles in inhomogeneous turbulence. J. Aerosol Sci. 14 (6), 729–739.
Reeks, M.W., 1992. On the continuum equations for dispersed particles in nonuniform flows. Phys. Fluids 4 (6), 1290–1303.
Reeks, M.W., 2005. On model equations for particle dispersion in inhomogeneous turbulence. Int. J. Multiph. Flow 31 (1), 93–114.
Reichhardt, V.H., 1951. Vollstiindige Darstellung- der turbulenten Geschwindigkeitsverteilung in glatten Leitungen. Z. angew. Math. Mech. 31 (7), 208–219.
Richardson, J.F., Zaki, W.N., 1954. Sedimentation and fluidisation. Part 1. Trans. Inst. Chem. Eng. 32, 35–53.
Rowe, P.N., 1987. A convenient empirical equation for estimation of the Richardson-Zaki exponent. Chem. Eng. Sci. 42, 2795–2796.
Saffman, P.G., 1965. The lift on a small sphere in a slow shear flow. J. Fluid Mech. 22 (2), 385–400.
Santos, D.S., Faia, P.M., Garcia, F.A.P., Rasteiro, M.G., 2019. Experimental and simulated studies of oil/water fully dispersed flow in a horizontal pipe. J. Fluids Eng. 141.
Santos, D., Garcia, F., Rasteiro, M., Faia, P., 2020. Oil/water flow in a horizontal pipe—dispersed flow regime. Int. J. Comp. Meth. Exp. Meas. 8 (2), 123–134.
Skartlien, R., 2007. Kinetic modeling of particles in stratified flow – Evaluation of dispersion tensors in inhomogeneous turbulence. Int. J. Multiph. Flow 33, 1006–1022.
Skartlien, R., 2009. A droplet transport model for channel and pipe flow based on particle kinetic theory and a stress–omega turbulence model International. J. Multiphase Flow 35, 603–616.
Skartlien, R., Nuland, S., Amundsen, J.E., 2011. Simultaneous entrainment of oil and water droplets in high Reynolds number gas turbulence in horizontal pipe flow. Int. J. Multiph. Flow 37, 1282–1293.
Soleimani, A., 1999. Phase distribution and associated phenomena in oil-water flows in horizontal tubes. Imperial College, London.
Sommerfeld, M., 1992. Modeling of Particle-Wall Collisions in Confined Gas-Particle Flows. Int. J. Multiph. Flow 18 (6), 905–926.
Stokes, G.G., 1851. On the effect of the internal friction of fluids on the motion of pendulums. Trans. Cambridge Philos. Soc. 9, 8–106.
Swailes, D.C., Reeks, M.W., 1994. Particle deposition from a turbulent flow. I. A steady-state model for high inertia particles. Phys. Fluids 6 (10), 3392–3403.
Taylor, G., 1954. The dispersion of matter in turbulent flow through a pipe. Proc. R. Soc. Lond. A 223, 446–468.
Tian, Z.F., 2006. Numerical modelling of turbulent gas-particle flow and Its applications. RMIT University.
Vames, J.S., Hanratty, T.J., 2004. Turbulent dispersion of droplets for air flow in a pipe. Exp. Fluids 6 (2), 94–104.
van Wijngaarden, T., 1976. Hydrodynamic interaction between gas bubbles in liquid. J. Fluid Mech. 77, 27–44.
Wachem, B.G.M.v., Schouten, J.C., Bleek, C.M.v.d., Krishna, R., Sinclair, J.L., 2001. Comparative analysis of CFD models of dense gas–solid systems. AIChE J. 46, 1035–1105.
Yang, J., Li, P., Zhang, X., Lu, X., Li, Q., Mi, L., 2021. Experimental investigation of oil–water flow in the horizontal and vertical sections of a continuous transportation pipe. Sci. Rep. 11 (1).
Young, J.B., Hanratty, T.J., 1991. Optical studies on the turbulent motion of solid particles in a pipe flow. J. Fluid Mech. 231, 665–688.
Yuan, Z., Michaelides, E.E., 1992. Turbulence modulation in particulate flows — A theoretical approach. Int. J. Multiph. Flow 18 (5), 779–785.